Lead-antimony sulfosalts from Tuscany (Italy). XVI. Carducciite, $(AgSb)Pb_6(As,Sb)_8S_{20}$, a new Sb-rich isotype of rathite from the Pollone mine, Valdicastello Carducci: occurrence and crystal structure

CRISTIAN BIAGIONI[1*], PAOLO ORLANDI[1], YVES MOËLO[2], LUCA BINDI[3]

[1] *Dipartimento di Scienze della Terra, Università di Pisa, Via S. Maria 53, I-56126 Pisa, Italy*
[2] *Institut des Matériaux Jean Rouxel, UMR 6502, CNRS, Université de Nantes, 2, rue de la Houssinière, 44 322 Nantes Cedex 3, France*
[3] *Dipartimento di Scienze della Terra, Università di Firenze, Via G. La Pira 4, I-50121 Firenze, Italy*

**e-mail address*: biagioni@dst.unipi.it

ABSTRACT

The new mineral species carducciite, $(AgSb)Pb_6(As,Sb)_8S_{20}$, has been discovered in the baryte-pyrite-(Pb-Ag-Zn) deposit of the Pollone mine, near Valdicastello Carducci, Apuan Alps, Tuscany, Italy. It occurs as black prismatic crystals, up to 0.5 mm in length, associated with pyrite and sterryite. Carducciite is opaque with a metallic luster and shows a black streak. It is brittle; the Vickers hardness (VHN_{10}) is 61 kg/mm^2 (range: 52 – 66), corresponding to a Mohs hardness of ~ 2½ – 3. In reflected light, carducciite is dark grey in colour, moderately bireflectant, and pleochroic from light grey to a slightly greenish grey. With crossed polars, it is anisotropic with grayish to light-blue rotation tints. Internal reflections are very weak and deep red in colour. Reflectance percentages for the four COM wavelengths are tabulated. Electron microprobe analysis gives (wt% – mean of 6 analyses): Ag 3.55(12), Tl 0.13(3), Pb 41.90(42), Sb 17.79(19), As 12.41(14), S 22.10(17), total 97.9(6). On the basis of $\Sigma Me = 16$ *apfu*, the chemical formula is $Ag_{0.96}Tl_{0.02}Pb_{5.91}As_{4.84}Sb_{4.27}S_{20.14}$. Main diffraction lines, corresponding to multiple *hkl* indices, are (relative visual intensity): 3.689 (s), 3.416 (s), 3.125 (s), 2.989 (s), 2.894 (s), 2.753 (vs), 2.250 (s). The crystal structure study gives a monoclinic unit cell, space group $P2_1/c$, with a 8.4909(3), b 8.0227(3), c 25.3957(9) Å, β 100.382(2)°, V 1701.63(11) Å^3, $Z = 2$. The crystal structure has been solved and refined to a final $R_1 = 0.063$ on the basis of 4137 observed reflections. It can be described in the frame of the sartorite homologous series, as formed by chemically twinned layers of the dufrénoysite type. The simplified structural formula is based on 20 sulfur atoms and can ideally be written as $(AgSb)Pb_6(As,Sb)_{\Sigma=8}S_{20}$. Carducciite is an (Ag,Sb)-rich homeotype of dufrénoysite, stabilized by the complete coupled substitution $2\ Pb^{2+} = Ag^{+} + Sb^{3+}$ on a specific site of the crystal structure. Together with barikaite, it belongs to the rathite isotypic series, whose crystal chemistry is discussed.

Keywords: carducciite, new mineral species, rathite series, sulfosalt, lead, antimony, arsenic, crystal structure, Pollone mine, Apuan Alps, Tuscany, Italy.

Introduction

During the last five years, a series of new or very rare Ag-Pb/Sb-As and Tl-Pb/Sb-As sulfosalts have been identified from the baryte-pyrite-iron oxide deposits of the southern Apuan Alps, Tuscany, Italy: sterryite, parasterryite, and meerschautite from the Pollone mine, near Valdicastello Carducci (Moëlo *et al*., 2011; Biagioni *et al*., 2013), boscardinite and protochabournéite from the Monte Arsiccio mine (Orlandi *et al*., 2012, 2013).

During a routine check of mineral samples from the Pollone mine, some crystals were preliminary identified as an Sb-rich variety of rathite (Biagioni *et al*., 2012). Rathite is a very rare Ag-(Tl)-Pb sulfosalt first described by Baumhauer (1896) from Lengenbach, Binntal, Switzerland. Recently, rathite was also identified from the dolostone outcrop of Reckibach, Binntal, Switzerland (Cannon *et al*., 2008). Consequently, Pollone mine could be the third natural occurrence of this sulfosalt, deserving a more accurate characterization. In addition, preliminary chemical analysis showed an unusual richness in antimony, a surprising feature given that rathite from Lengenbach shows only minor Sb. Consequently, a crystallographic study was performed, which showed the peculiar crystal-chemical role played by Sb.

Crystallographic study, chemical analysis, and crystal-chemical considerations point to the distinction between rathite and this Sb-rich isotype, which was named carducciite. The mineral and its name have been approved by the CNMNC-IMA, under the number 2013-006. The holotype specimen of carducciite is deposited in the mineralogical collection of the Museo di Storia Naturale, Università di Pisa, Via Roma 79, Calci, Pisa, Italy, under catalog number 19646. The name is for the type locality, Valdicastello Carducci. This is the type locality of other two sulfosalts, parasterryite (Moëlo *et al*., 2011) and meerschautite (Biagioni *et al*., 2013). The name also remembers the family name Carducci: the Italian poet Giosué Carducci (1835-1907), Nobel Prize winner for literature in 1906, was born at Valdicastello. His father, Michele (1808-1858), was employed as a doctor at the Pollone Pb-Ag mine from 1833 to 1836.

After the submission of the approval proposal of carducciite to the CNMNC-IMA, we became aware of the approval of barikaite (Topa *et al*., 2013), a closely but distinct related phase, found in the Barika Au-Ag deposit, Azarbaijan Province, western Iran. In this paper we describe carducciite from the baryte-pyrite-(Pb-Zn-Ag) deposit of Pollone, Valdicastello Carducci, and its relationship with rathite and barikaite.

Geological setting

The baryte-pyrite-(Pb-Ag-Zn) deposit of Pollone (latitude 43°57’ N; longitude 10°16’ E) is located in the southern portion of the Sant’Anna tectonic window, an area in which metamorphic rocks are surrounded by the non-metamorphic sedimentary formations of the Tuscan Nappe. The deposit is hosted in the Scisti di Fornovolasco Formation, belonging to the Fornovolasco-Panie Unit. This formation is related to the Variscan basement of the Apuan Unit (Pandeli *et al*., 2004) and is composed by a Paleozoic – Early Triassic (?) metavolcanic-metasedimentary sequence metamorphosed to the greenschist *facies*. During the late-stages of the Alpine orogeny, the development of shear zones led to the formation of numerous quartz + baryte veins; fluids were focused along these shear zones giving rise to syn-metamorphic and syn-tectonic veins. Estimates of *P–T* conditions indicate that host and country rocks record metamorphic temperatures and pressure of about 350°C and 0.35 GPa, respectively;

appreciably higher temperatures (around 450°C) were found for the mineralizing fluids (Costagliola *et al.*, 1998).

A great variety of sulfosalts have been described from all the baryte-pyrite-iron oxide deposits from the southern Apuan Alps (Table 1), and in particular from the Buca della Vena, Monte Arsiccio, and Pollone mines. It is interesting to note that every deposit has some chemical peculiarities. Indeed, Buca della Vena mine is characterized by the occurrence of oxy-sulfosalts and oxy-chloro-sulfosalts; the Monte Arsiccio mine is particularly attractive for the occurrence of thallium sulfosalts, and the Pollone mine shows the presence of complex silver-lead sulfosalts. Carducciite is one of these rare mineral species.

Occurrence and mineral description

Physical and optical properties

Carducciite has been identified in only few specimens from the Pizzone stope, in an area rich of acicular sulfosalts. Carducciite was observed embedded in the saccharoidal baryte or rarely in small vugs, as black prismatic crystals, striated parallel to the elongation, up to 0.5 mm long and 0.2 mm in width (Fig. 1). It is brittle, with a conchoidal fracture. Streak is black and luster is metallic.

Micro-indentation measurements carried out with a VHN load of 10 g give a mean value of 61 kg/mm^2 (range: 52 – 66) corresponding to a Mohs hardness of about 2½ – 3.

In plane-polarized incident light, carducciite is dark grey in colour, moderately bireflectant, and pleochroic from light grey to a slightly greenish grey. Between crossed polars, carducciite is anisotropic with greyish to light-blue rotation tints. Internal reflections are very weak and deep red in colour. There is no optical evidence of growth zonation.

Reflectance measurements were performed in air by means of a MPM-200 Zeiss microphotometer equipped with a MSP-20 system processor on a Zeiss Axioplan ore microscope. The filament temperature was approximately 3350 K. An interference filter was adjusted, in turn, to select four wavelengths for measurement (471.1, 548.3, 586.6, and 652.3 nm). Readings were taken for specimen and standard (SiC) maintained under the same focus conditions. The diameter of the circular measuring area was 0.1 mm. Reflectance percentages for R_{min} and R_{max} are 35.8, 40.8 (471.1 nm), 33.7, 39.0 (548.3 nm), 32.7, 37.6 (586.6 nm), and 30.4, 35.1 (652.3 nm), respectively.

Owing to its softness and fragility, only minute grains could be extracted from baryte for X-ray study and preparation as polished sections for microprobe analysis and reflectance measurement. These grains were unsuitable for measuring the density. Calculated density (based on the empirical formula) is 5.559 g/cm^3.

Carducciite is associated with baryte, pyrite, sphalerite, sterryite, and twinnite. Up to now, only few submillimeter-sized fragments of carducciite have been identified; it is probably the rarest sulfosalts so far found at the Pollone mine.

Chemical analysis

A crystal of carducciite was analyzed with a CAMEBAX SX50 electron microprobe (BRGM-CNRS-University common laboratory, Orléans, France). The operating conditions were: accelerating voltage 20 kV, beam current 20 nA, beam size 5 μm. Standards (element,

emission line, counting times for one spot analysis) are: pyrite (S *K*α, 20 s), stibnite (Sb *L*α, 20 s), AsGa (As *L*α, 30 s), Ag metal (Ag *L*α, 20 s), galena (Pb *M*α, 20 s), and lorandite (Tl *M*α, 20 s).

Electron microprobe data for carducciite are given in Table 2. Notwithstanding the low total, probably due to the bad quality of the polished surface, the results are in agreement with the structural analysis (see below). On the basis of Σ*Me* = 16 atoms per formula unit (*apfu*), the chemical formula can be written as $Ag_{0.96(3)}Tl_{0.02(1)}Pb_{5.91(4)}(As_{4.84(4)}Sb_{4.27(6)})_{\Sigma=9.11}S_{20.14(14)}$. If Tl and Ag are subtracted according to the substitution rule $(Tl,Ag)^{+} + (As, Sb)^{3+} = 2\ Pb^{2+}$, the chemical formula can be written $Pb_{7.87}(As,Sb)_{\Sigma=8.13}S_{20.14(14)}$, agreeing with the general formula of the N = 4 dufrénoysite homologue of the sartorite series (Makovicky, 1985), $Pb_8As_8S_{20}$.

Crystallography

The X-ray powder diffraction pattern of carducciite was obtained using a 114.6 mm diameter Gandolfi camera, with Ni-filtered Cu *K*α radiation. The observed X-ray powder pattern is compared with the calculated one (obtained using the software *PowderCell*; Kraus and Nolze, 1996) in Table 3. Unit-cell parameters were not refined from the X-ray powder diffraction data because of the multiplicity of indices for the majority of the diffraction lines.

For the X-ray single-crystal study, the intensity data were collected using a Bruker Smart Breeze diffractometer equipped with an air-cooled CCD detector, with Mo *K*α radiation. The detector to crystal distance was 50 mm. 878 frames were collected using ω scan mode, in 0.5° slices, with an exposure time of 10 seconds per frame. The data were corrected for the Lorentz and polarization factors and absorption using the package of software *Apex2* (Bruker AXS Inc., 2004). The statistical tests on the distribution of $|E|$ values ($|E^2-1| = 0.868$) and the systematic absences suggested the space group $P2_1/n$, which was subsequently transformed by the matrix **R** = (1 0 0, 0 $\bar{1}$ 0, $\bar{1}$ 0 $\bar{1}$), into the standard setting $P2_1/c$. The refined cell parameters, in the standard setting, are *a* 8.4909(3), *b* 8.0227(3), *c* 25.3957(9) Å, β 100.382(2)°, *V* 1701.63(11) $Å^3$.

The crystal structure was refined using *Shelx-97* (Sheldrick, 2008) starting from the atomic coordinates given by Berlepsch *et al*. (2002). Scattering curves for neutral atoms were taken from the *International Tables for X-ray Crystallography* (Wilson, 1992). Crystal data and details of the intensity data collection and refinement are reported in Table 4. After several cycles of isotropic refinement, the R_1 converged to 0.14; by refining the anisotropic displacement parameters for the metals only, the refinement yielded a R_1 value of 0.074, thus confirming the correctness of the structural model. Successive cycles of refinement converged to $R_1 = 0.071$, with an anisotropic model for all the atoms. The M5 site was found to split in two positions (*i.e*., M5a and M5b). The refinement of the occupancy factors at these sites (using Sb *versus* structural vacancy) led to 24.7 and 24.2 electrons, respectively. The examination of bond distances suggests that M5a is occupied by a larger cation as Ag, whereas M5b by Sb. The successive refinement cycles were carried out using Ag *vs* vacancy (M5a) and Sb *vs* vacancy (M5b) lowers the R_1 to 0.069, and gave an overall composition for the M5 site of $Ag_{0.53}Sb_{0.47}$, in good agreement with the expected value. Finally, the occupancies were refined for M2, M3, M4 (As *vs* Sb) and M6 (Pb *vs* As).

According to Marumo and Nowacki (1965), rathite ("rathite I" of these authors), isotypic with carducciite (see below), is usually polysynthetically twinned. To verify such pseudo-merohedral twinning, the twin law ($\bar{1}$ 0 0, 0 $\bar{1}$ 0, 1 0 1) was added in the refinement but no improvement was found, thus indicating that the studied crystal is actually untwinned. Notwithstanding the observation of Marumo and Nowacki (1965), Berlepsch *et al*. (2002), through single-crystal X-ray diffraction data, Pring (2001), through high-resolution transmission electron microscopy, and Topa *et al*. (2013), through reflected light microscopy, did not observe any twinning in rathite and isotypic barikaite, respectively.

The refinement finally converged to $R_1 = 0.063$ for 4137 reflections with $F_o > 4\sigma(F_o)$ and 0.103 for all 6078 independent reflections. The highest and deepest residuals are located around Pb2 site. Atomic coordinates and bond distances are reported in Table 5 and Table 6, respectively, and the unit-cell content with atom labels is given in Fig. 2. Bond valence sums are given in Table 7.

The crystal-chemical formula of carducciite, as obtained through this refinement of the crystal structure, is $Ag_{1.05}Pb_{5.84}As_{4.63}Sb_{4.48}S_{20}$, with the relative error on the valence equilibrium Ev = +0.15. This formula is not exactly charge balanced, but it does not take into account the limited Pb for Tl substitution, which has not been localized, due to the very similar scattering factors of these two elements. In addition, it shows a slightly greater $Sb/(Sb+As)_{at.}$ ratio with respect to the results of chemical analysis, *i.e*. 0.49 *versus* 0.47.

Crystal structure description

General organization of carducciite

Figure 3 presents the general organization of the crystal structure of carducciite. It belongs to the N = 4 homologue of the sartorite series and it shows homeotypic relationship with dufrénoysite (Moëlo *et al*., 2008; Table 8). It can be described as formed by chemically twinned layers of the dufrénoysite type.

The crystal structure of rathite (as well as that of barikaite) displays walls of "standing" tricapped trigonal coordination prisms of Pb (prism axis parallel to **a**), alternating with slabs (dufrénoysite layers) composed of "lying" trigonal coordination prism of (As,Sb) and Pb, based on SnS archetype (Berlepsch *et al*., 2002). The structure of carducciite is basically similar to that described by Marumo and Nowacki (1965) and Berlepsch *et al*. (2002) for rathite from Lengenbach, and by Makovicky and Topa (2013) for barikaite. The walls of "standing" tricapped trigonal prisms, centered by Pb atoms (and possibly minor thallium) are formed by columns composed by the alternation, along **a**, of Pb1 and Pb2 polyhedra sharing faces. Adjacent columns are connected along **b** through edge-sharing, giving rise to the walls. Between the walls, dufrénoysite layers (N = 4) occur.

The dufrénoysite layer type occurs in different sulfosalts belonging to the sartorite homologous series: dufrénoysite, rathite, barikaite, liveingite, baumhauerite, baumhauerite-2*a*, and boscardinite. In carducciite, within the dufrénoysite layer, there are two pure (or nearly pure) As (M1) and Sb (M3) sites, two mixed (As,Sb) sites (M2 and M4, with As > Sb), and two split sites, *i.e*. an Ag/Sb split site (M5) and a Pb/As one with Pb > As (M6). Such an equivalent (Ag,Sb) and (Pb,As) pair is in the same configuration of the constitutive layer of

rathite, barikaite (in both phases, however, the split site M5 is occupied by Ag and As) and, in particular, of boscardinite (Orlandi *et al*., 2012).

Cation coordination and site occupancies

The crystal structure of carducciite contains two pure Pb sites, four Me^{3+} sites [where *Me* is As, Sb, or a (As,Sb)], two split sites (an Ag/Sb and a Pb/As site) and 10 S sites (Table 5). Pb1 and Pb2 are "standing" tricapped trigonal coordination prisms, with average bond-lengths of 3.188 and 3.205 Å, respectively. The four sites hosting As and/or Sb can be divided into two mixed (As,Sb) sites, a nearly pure As site, and a pure Sb site.

M1 site, with a mean bond length of 2.27 Å (in good agreement with rathite of Berlepsch *et al*., 2002 and barikaite, ***i.e.*** 2.26 and 2.28 Å, respectively) and a three-fold coordination, is a nearly pure As site; the refinement of its site occupancy indicates only a very minor Sb substitution (only 0.02 *apfu* Sb). The coordination is completed by two additional bonds at ~ 3.2 Å.

M2 and M4 sites are mixed (As,Sb) sites, with refined site occupancy $As_{0.60}Sb_{0.40}$ and $As_{0.66}Sb_{0.34}$, respectively. M2 has a three-fold coordination, with additional longer bonds at 2.9 and 3.3 Å; a similar coordination is shown by M4, with three shorter bonds and two longer ones, at 3.1 and 3.3 Å. According to Berlepsch *et al*. (2002) and considering only the bonds with *Me*–S distance lower than 2.70 Å, M2 and M4 of rathite are pure As sites, with average bond-lengths of 2.31 and 2.27 Å, respectively, to be compared with 2.39 and 2.35 Å of carducciite. In the crystal structure of barikaite, the M2 and M4 sites are labeled *Me*2 and *Me*3, respectively, and are mixed split (As,Sb) sites; according to Makovicky and Topa (2013), the split sub-positions points to $As_{0.55}Sb_{0.45}$ for *Me*2 site and $As_{0.82}Sb_{0.18}$ for *Me*3.

M3 is a pure Sb site, as indicated by the refinement of As *vs* Sb site-scattering value. Its average bond distance is 2.61 Å; M3 has two short bonds (2.44 and 2.46 Å) and two longer additional bonds (2.75 and 2.80 Å). This bond distribution is similar to that found by Berlepsch *et al*. (2002) for the split M3b position of rathite, which is occupied by arsenic; these authors reported two short bonds at 2.24 and 2.28 Å and two long bonds, at 2.69 and 2.73 Å. Whereas in rathite M3 is split into two sub-positions (M3a and M3b, occupied by $Sb_{0.265}$ and $As_{0.735}$, respectively), in carducciite there are no hints of such a splitting. In the crystal structure of barikaite, the M3 site is labeled as *Me*4 (Makovicky and Topa, 2013), and shows the same identical features observed in carducciite, that is a pure Sb occupancy and the same bond pattern, with an average bond distance of 2.61 Å.

The two split sites, M5 and M6, are occupied respectively by Ag/Sb and Pb/As. The splitting of the M5 site was proposed by Marumo and Nowacki (1965), with Ag in the M5a sub-site (s.o.f. 0.57), and As in M5b (s.o.f. 0.402). This was confirmed by Berlepsch *et al*. (2002), with the Ag(M5a)/As(M5b) = 0.474/0.526; in barikaite, the Ag/As ratio is 0.53/0.47 (Makovicky and Topa, 2013). In carducciite, M5a hosts Ag (s.o.f. 0.526), with a distorted octahedral coordination and average-bond-length of 2.80 Å, in agreement with 2.77 Å observed by Berlepsch *et al*. (2002) for rathite and by Makovicky and Topa (2013) for barikaite. On the contrary, whereas the three-fold coordinated M5b positions of rathite and barikaite studied by these authors show a mean bond distance of 2.38 and 2.39 Å, respectively, the average bond distance of M5b observed in carducciite is significantly larger,

i.e. 2.49 Å, ranging from 2.45 to 2.57 Å. Average bond distance and refined electron density at the M5b sub-position agree with an occupancy by Sb (s.o.f. 0.474). M6 site is split into two sub-positions, namely M6a and M6b, hosting respectively Pb (s.o.f. 0.92) and minor As (s.o.f. 0.08). M6a is a "lying" monocapped trigonal prism, with average bond length of 3.04 Å. As pointed out also by Berlepsch *et al*. (2002), the coordination of M6b is not characteristic of arsenic, having four bonds ranging between 2.53 and 2.82 Å, and two longer bonds up to 3.53 Å. Probably, owing to the very low occupancy of the site, the exact positions of the associated S ligands cannot be resolved. Makovicky and Topa (2013) observed, for barikaite, the splitting of the M6 site into three sub-positions, namely Ag6, Pb6, and Sb6, with s.o.f. 0.28, 0.43, and 0.29, respectively.

Polymerization of $Me^{3+}S_3$ triangular pyramidal polyhedra

Marumo and Nowacki (1965) pointed that in rathite "AsS_3 pyramids form chains with finite lengths", *i.e.* As_mS_n polymers. Reexamination of the structure indicates two possible combinations of two polymers, 1) $As_3S_7 + As_6S_{13}$, or 2) $As_5S_{11} + As_4S_9$. Refinement of the structure by Berlepsch *et al*. (2002) shows the validity of choice 2) (we do not take into account the mixed (Pb,As) M6 position). Such a polymeric organization was later recognized in various lead sulfosalts: andorite VI (Sawada *et al*., 1987), sartorite (Berlepsch *et al*., 2003), boscardinite (Orlandi *et al*., 2012), and the pair sterryite/parasterryite (Moëlo *et al*., 2012).

In carducciite, if only the shortest (= strongest) Me^{3+}–S bonds are considered (below 2.70 Å – see Moëlo *et al*., 2012), "reduced" $(Sb/As)S_3$ triangular pyramidal polyhedra appear. The only exception is represented by M3 site, which has only two bonds shorter than 2.70 Å; however, the third and fourth bonds (M3–S9 and M3–S8) are only a little longer, being ~ 2.75 and 2.80 Å, respectively. The projection perpendicular to **a** of one oblique ribbon of the dufrénoysite type (Fig. 4a) reveals in this way the oblique stacking (~ 45° relatively to the elongation) of finite 1D units elongated along $[100]_{PbS}$, with the ideal formula of carducciite, more exactly $AgPb_6Sb_3(As,Sb)_4As_2S_{20}$ (taking M6 = pure Pb, M1 = pure As, and M5a = M5b = 0.50). Without Ag and Pb, $(Sb/As)S_3$ polyhedra constitute a single $Sb_3(As,Sb)_4As_2S_{20}$ polymer (Fig. 4b – No. 1).

Nevertheless, in this polymer the M3 position appears to be a mean position, due to the long M3–S9 and M3–S8 bonds. Thus, when one of the two M3 positions is bound to S9, the second one must be bound to S8. Two choices are possible (Fig. 4b – No 2 and 3), but choice No 2 seems the most probable. Indeed, there is a dissymmetry in the two M5b–M3 distances, a short one (3.60 Å), and a long one (3.89 Å). In choice No 3, the shift of M3 towards S9 will shorten the M5b–M3 distance below 3.60 Å, and thus increases the repulsion between these two Sb atoms. This is not the case in choice No 2, which appears more favourable from the energetic point of view. Considering this choice, the ordered structure would correspond to the combination of two polymers, $(As,Sb)_2AsS_7$ and $Sb_3(As,Sb)_2AsS_{13}$.

Crystal chemistry of the rathite isotypic series

Carducciite: a homeotypic derivative of dufrénoysite

The main characteristic of the crystal structure of carducciite is its derivation from the dufrénoysite pole by the complete coupled substitution $2Pb^{2+} = Ag^{+} + Sb^{3+}$ at the M5 position.

This substitution is a case of valency-imposed double site-occupancy (Hatert and Burke, 2008). An equivalent substitution, with As assuming the role of Sb, occurs in rathite as well as in barikaite and this is also required for the stability of these two phases relatively to dufrénoysite. Such a coupled substitution lead to a space group ($P2_1/c$) distinct from that of dufrénoysite ($P2_1$): carducciite is a homeotype of dufrénoysite.

The rathite isotypic series

Carducciite is isotypic with rathite. It constitutes a specific mineral species, and not simply an Sb-rich variety of rathite, because the specific structural role played by Sb^{3+}, instead of As^{3+}, at the M5 position. Barikaite is also isotypic with rathite. Its $P2_1/n$ setting is also that of rathite (Topa *et al*., 2013), and can be conveniently transformed into the conventional $P2_1/c$ setting through the transformation matrix **R** = (1 0 0, 0 $\bar{1}$ 0, $\bar{1}$ 0 $\bar{1}$), as suggested by Berlepsch *et al*. (2002).

These relationships permit to define the rathite isotypic series. In Table 8 are reported the cell constants of rathite, carducciite, and barikaite in the $P2_1/c$ setting. Thus, there is no change in the symmetry of the unit cell which would allow to discriminate barikaite from rathite or carducciite.

Crystal chemical substitutions in the rathite series

Table 9 reports available chemical data of rathite and barikaite. Another chemical analysis of rathite was reported by Nowacki and Bahezre (1963) but actually it did not represent rathite, owing to the absence of Ag, contrasting with the structure solution of Marumo and Nowacki (1965) indicating the occurrence of this element as an essential component. Consequently, this chemical data will not be accounted for.

Figure 5 shows the Pb content *versus* (Sb + As) content (Fig. 5a) and Ag (Fig. 5b); Pb and (Sb + As) contents have been corrected subtracting Tl. In the framework of the N = 4 homologues of the sartorite series, rathite and carducciite correspond to phases having $x = 1$, with ideal composition $AgPb_6(As,Sb)_9S_{20}$. As stressed above, these two minerals differ from dufrénoysite, the chemical pole with $x = 0$ and chemical formula $Pb_8As_8S_{20}$, for the coupled substitution $Ag^+ + Me^{3+} = 2\ Pb^{2+}$. Consequently, following Berlepsch *et al*. (2002), the chemical formula of rathite and carducciite could conveniently be written as $(AgAs)Pb_6(As,Sb)_8S_{20}$ and $(AgSb)Pb_6(As,Sb)_8S_{20}$, respectively. Barikaite is close to the chemical pole having $x = 1.5$, $Ag_{1.5}Pb_5(As,Sb)_{9.5}S_{20}$; its crystal chemical formula may be written $Ag_{0.5}(AgAs)Pb_5(As,Sb)_{8.5}S_{20}$. The tie-lines in Figure 5 represent the substitution $Me^+ + Me^{3+} = 2\ Me^{2+}$ between dufrénoysite, $Pb_8As_8S_{20}$, and the hypothetical ideal endmember composition $Ag_2Pb_4(As,Sb)_{10}S_{20}$. In this homeotypic series, starting from the dufrénoysite pole, three kinds of substitution occur:

i) the homovalent substitution $As^{3+} = Sb^{3+}$;

ii) the double substitution $2Pb^{2+} = Me^{3+} + Ag^+$;

iii) the double substitution $2Pb^{2+} = Tl^+ + Me^{3+}$.

The first substitution takes place in particular at the M3 site and, in minor amounts, at the M2 and M4 sites. In particular, M3 site has a refined site-occupancy ($As_{0.74}Sb_{0.26}$) in rathite from Lengenbach (Berlepsch *et al*., 2002), whereas it is a pure Sb site in carducciite

and barikaite. Indeed, carducciite and barikaite are richer in Sb than rathite, with an $Sb/(Sb+As)_{at.}$ ratio of 0.47 and 0.42 for carducciite and barikaite, respectively, to be compared with values ranging between 0 and 0.07 for rathite (Table 10).

The second substitution involves the M5 site and it is required for the stability of rathite, barikaite, and carducciite with respect to dufrénoysite. The peculiar crystal chemical role of silver in rathite was revealed by the crystal structure study of Marumo and Nowacki (1965), refined by Berlepsch *et al*. (2002). It was enhanced by the EPMA data of Laroussi *et al*. (1989). The trivalent Me^{3+} cation could be As in rathite and barikaite and Sb in carducciite. Barikaite shows an Ag excess hosted at the M6 site; the introduction of the Ag excess is ruled by this same second kind of substitution.

Finally, rathite from Lengenbach has a variable thallium content, ranging between 0.28 and 1.35 *apfu*. Carducciite and barikaite are quite Tl-free, showing only 0.13 and 0.15 wt% Tl (detection limit, for carducciite analysis, 0.07 wt%), corresponding to 0.04 *apfu* in both species. Thallium shows a clear negative correlation with lead and actually carducciite is richer in lead than rathite (11.82 *apfu*, whereas the values for rathite from Lengenbach ranges between 9.10 and 11.70 *apfu*). Thallium should be hosted at the Pb1 and/or Pb2 sites, in agreement with its typical nine-fold coordination in other sulfosalts, *e.g*., boscardinite (Orlandi *et al*., 2012). If thallium occurs, then M6 is occupied by Me^{3+} cations, whereas if thallium is absent, M6 is occupied by lead. This is in agreement with experimental data that indicate, for thallium-bearing rathite from Lengenbach, a site occupancy $Pb_{0.74}As_{0.26}$, corresponding to 1.04 As *pfu*. On the contrary, refining Pb *vs* As at the M6 split site of carducciite, a site occupancy $Pb_{0.91}As_{0.09}$ was achieved, corresponding to 0.36 *apfu*, in agreement with a minor importance of the $2Pb^{2+} = Tl^{+} + Me^{3+}$ substitution. In addition, it is not clear if Me^{3+} is preferentially arsenic or antimony. In fact, the bond distances for the M6b split site in rathite and carducciite are not usual for arsenic in trigonal pyramid coordination. According to Berlepsch *et al*. (2002) it could be due to the low site-occupancy of this position, and the consequent impossibility of resolving the S disorder associated with the Pb–As substitution. However, it could not be excluded the possibility of a Pb–Sb substitution, as observed in other phases of the sartorite homologous series and particularly in boscardinite (Orlandi *et al*., 2012) and barikaite (Makovicky and Topa, 2013). Moreover, chemical data for rathite from Lengenbach indicates the existence of a Tl-bearing variety of rathite, containing about 1 Tl *pfu*, and a Tl-poor variety, hosting less than 0.55 *apfu* of thallium (Table 9). It is noteworthy that the former shows about 1 *apfu* of Sb, whereas in the latter Sb is scarce or absent. Actually, as exemplified by barikaite, the M6 site is quite flexible, being able to host Pb^{2+}, As^{3+}, Sb^{3+}, as well as Ag^{+}.

Distinction between carducciite, barikaite, and rathite

Carducciite has been defined as a distinct species relatively to rathite on the sole basis of the filling of the M5 site, *i.e*. Ag + Sb, against Ag + As in rathite. The high Sb concentration substituting on the As sites was not considered, as the $Sb/(As+Sb)_{at.}$ ratio is below 50% limit in a binary solution. Thus, the limit between carducciite and rathite would correspond to the 50% limit within the M5 position, *i.e*. $(Ag_{0.50}Sb_{0.25}As_{0.25})$.

On the contrary, Topa *et al*. (2013) point the ordered distribution of As and Sb among pure (As,Sb) sites in barikaite, that "represents a feature which separates it from rathite". They

conclude that "barikaite is a homeotype of the pure arsenian N = 4 member of the sartorite homologous series, rathite". This description of barikaite as a homeotype of rathite contradicts unit-cell and crystal structure data, which demonstrate their isotypie: same type of unit cell, same space group, exact topological correspondence between cation as well as sulfur sites, without any difference (vacancy or interstitial). In the modular description of barikaite structure, Makovicky and Topa (2013) take into account the shortest (As,Sb)–S bonds to distinguish finite crank-shaft chains (*i.e*. $(As,Sb)_mS_n$ polymers as indicated above), whose sizes are different from those observed in rathite. It is this difference, together with As/Sb ordering, which justifies in their eyes the homeotypic derivation of barikaite from rathite. But such a polymeric description, without any consequence on the crystallographic characteristics (despite the Sb-enrichment of barikaite), omits longest (As,Sb)–S bonds. Taking into account all S ligands, polyhedra around all (As,Sb) positions are topologically identical between barikaite and rathite. Barikaite and rathite are isotypic, not homeotypic.

In barikaite, the $Sb/(As+Sb)_{at.}$ ratio of pure (As,Sb) sites is 0.41, clearly below the 50% limit; it would not justify its distinction from rathite. On the contrary, a specific feature of barikaite is the substitution of (Ag+Sb) to 2Pb at the M6 site, over the 50% limit (56%). This could be taken as the criterium for the definition of barikaite relatively to rathite, as well as carducciite. On this basis, the structural formulas for the rathite isotypic series would be (Σ *Me* = 16 *apfu*):

i) rathite (low Ag, Sb low or absent): $^{M5}(AgAs)^{M6}Pb_2Pb_4(As,Sb)_8S_{20}$;

ii) barikaite (high Ag, high Sb): $^{M5}(AgAs)^{M6}(Ag_{0.5+x}Sb_{0.5+x}Pb_{1-2x})Pb_4(As,Sb)_8S_{20}$ ($0 < x < 0.5$);

iii) carducciite (low Ag, higher Sb): $^{M5}(AgSb)^{M6}Pb_2Pb_4(As,Sb)_8S_{20}$.

Relationship with sterryite and parasterryite

During the study of sterryite and parasterryite, Moëlo *et al*. (2011) noted that in the pseudoternary system Pb_2S_2-$(Sb,As)_2S_3$-$(Ag,Cu)_2S$, the chemically closest sulfosalts are the owyheeite solid-solution field and rathite. Owyheeite was previously reported from the Pollone mine by Carmignani *et al*. (1976) on the basis of electron-microprobe data. Carducciite occurs in the same assemblage than sterryite; it is noteworthy that Moëlo *et al*. (2011) underlined that parasterryite can be considered a perfect mixture of owyheeite and Tl-free rathite. As discussed in this paper, carducciite is the Sb-rich, Tl-free isotype of rathite, and appears more appropriate as the As-rich component, together with owyheeite, of the sterryite "mixture".

The occurrence of such sulfosalts (Table 10) indicates the great potentiality of the Pollone mine for the study of the paragenetic relationships between Ag-sulfosalts. At Pollone, these phases are the result of reactions and recrystallizations during Alpine metamorphism. Up to now, carducciite was observed only embedded in the granoblastic baryte, whereas sterryite and parasterryite occurs also in late-stage cavities. However, a detailed study of the textural relationship between these phases is necessary to understand the evolution of the hydrothermal system at Pollone mine.

Conclusion

438 The occurrence of carducciite from the Pollone mine brings useful new data for the
439 knowledge of the sartorite homologous series and for the phase equilibria in the PbS-Ag_2S-
440 As_2S_3-Sb_2S_3 system. The richness in antimony of carducciite with respect to rathite agrees
441 with the usual crystal-chemistry of lead sulfosalts from Apuan Alps. Sb-rich analogues or
442 varieties of arsenic sulfosalts were described, for example, from the Monte Arsiccio mine, *i.e*.
443 boscardinite, the Tl-Sb homeotype of baumhauerite, and protochabournéite (Orlandi *et al*.,
444 2012, 2013).
445 The crystal chemistry of the dufrénoysite homeotypic series points to several questions
446 which must be clarified. The crystal structure of veenite, the Sb-rich derivative of
447 dufrénoysite (Jambor, 1967) must be resolved, in order to examine the distribution of Sb
448 among primitive As positions of dufrénoysite. In the rathite isotypic sub-series, there is a
449 competition starting from rathite between the Sb enrichment, which favours the incorporation
450 of Sb at the M5 position, and the Ag enrichment, which maintains As at the M5 position, but
451 promotes Sb incorporation at the M6 position. The limit between these two very close trends,
452 which determines the distinction between barikaite and carducciite, remains unknown.
453 Another question is the limit between rathite and carducciite, i.e. what is the Sb/As ratio in the
454 solid solution controlling the ($Ag_{0.50}Sb_{0.25}As_{0.25}$) limit on the M5 position?
455

456 ## Acknowledgements

457 Electron microprobe analyses were performed with the help of O. Rouer (CNRS engineer,
458 Institut des Sciences de la Terre d'Orléans).
459

References

Baumhauer, H. (1896) Ueber den Rathit, ein neues mineral aus dem Binnenthaler Dolomit. *Zeitschrift für Kristallographie*, **26**, 593–602.

Berlepsch, P., Armbruster, T. and Topa, D. (2002) Structural and chemical variations in rathite, $Pb_8Pb_{4-x}(Tl_2As_2)_x(Ag_2As_2)As_{16}S_{40}$: modulations of a parent structure. *Zeitschrift für Mineralogie*, **217**, 581–590.

Berlepsch, P., Armbruster, T., Makovicky, E. and Topa, D. (2003) Another step toward understanding the true nature of sartorite: determination and refinement of a ninefold superstructure. *American Mineralogist*, **88**, 450–461.

Biagioni, C., Orlandi, P., Moëlo, Y., Pardini, S. and Passarino, G. (2012) Sterryite e parasterryite. I solfosali aciculari di piombo e argento della miniera del Pollone (Pietrasanta, Lucca). *Rivista Mineralogica Italiana*, **2/2012**, 76–91.

Biagioni, C., Moëlo, Y., Orlandi, P., Stanley, C.J. and Evain, M. (2013) Meerschautite, IMA 2013-061. CNMNC Newsletter No. 17, October 2013, page 3004. *Mineralogical Magazine*, **77**, 2997–3005.

Brese, N.E. and O'Keeffe, M. (1991) Bond-valence parameters for solids. *Acta Crystallographica*, **B47**, 192–197.

Bruker AXS Inc. (2004) APEX 2. Bruker Advanced X-ray Solutions, Madison, Wisconsin, USA.

Cannon, R., Hensel, H. and Raber, T. (2008) Der Reckibach-Dolomit im Binntal, Schweiz: Mineralbestand und Neufunde. *Lapis*, **33**, 20–28.

Carmignani, L., Dessau, G. and Duchi, G. (1976) I giacimenti a barite, pirite ed ossidi di ferro delle Alpi Apuane. Studio minerogenetico e strutturale. *Bollettino della Società Geologica Italiana*, **95**, 1009–1061.

Costagliola, P., Benvenuti, M., Lattanzi, P. and Tanelli, G. (1998) Metamorphogenic barite-pyrite (Pb-Zn-Ag) veins at Pollone, Apuane Alps, Tuscany: vein geometry, geothermobarometry, fluid inclusions and geochemistry. *Mineralogy and Petrology*, **62**, 29–60.

Hatert, F. and Burke, E.A.J. (2008) The IMA-CNMNC dominant-constituent rule revisited and extended. *Canadian Mineralogist*, **46**, 717–728.

Jambor, J.L. (1967) New lead sulfantimonides from Madoc, Ontario – Part 1. *Canadian Mineralogist*, **9**, 7–24.

Laroussi, A., Moëlo, Y., Ohnenstetter, D. and Ginderow, D. (1989) Argent et thallium dans les sulfosels de la série de la sartorite (Gisement de Lengenbach, vallée de Binn, Suisse). *Comptes Rendus de l'Académie des Sciences, Paris*, **308**, Série II, 927–933.

Makovicky, E. (1985) The building principles and classification of sulphosalts based on the SnS archetype. *Fortschritte der Mineralogie*, **63**, 45–89.

Makovicky, E. and Topa, D. (2013) The crystal structure of barikaite. *Mineralogical Magazine*, **77**, 3093–3104.

Marumo, F. and Nowacki, W. (1965) The crystal structure of rathite-I. *Zeitschrift für Kristallographie*, **122**, 433–456.

Marumo, F. and Nowacki, W. (1967) The crystal structure of dufrenoysite, $Pb_{16}As_{16}S_{40}$. *Zeitschrift für Kristallographie*, **124**, 409–419.

Moëlo, Y., Makovicky, E., Mozgova, N.N., Jambor, J.L., Cook, N., Pring., A., Paar, W.H., Nickel, E.H., Graeser, S., Karup-Møller, S., Balić-Žunić, T., Mumme, W.G., Vurro, F., Topa, D., Bindi, L., Bente, K. and Shimizu, M. (2008) Sulfosalt systematics: a review. Report of the sulfosalt sub-committee of the IMA Commission on Ore Mineralogy. *European Journal of Mineralogy*, **20**, 7–46.

Moëlo, Y., Orlandi, P., Guillot-Deudon, C., Biagioni, C., Paar, W. and Evain, M. (2011) Lead-antimony sulfosalts from Tuscany (Italy). XI. The new mineral species parasterryite, $Ag_4Pb_{20}(Sb_{14.5}As_{9.5})_{\Sigma 24}S_{58}$, and associated sterryite, $Cu(Ag,Cu)_3Pb_{19}(Sb,As)_{\Sigma 22}(As–As)S_{56}$, from the Pollone mine, Tuscany, Italy. *Canadian Mineralogist,* **49**, 623–638.

Moëlo, Y., Guillot-Deudon, C., Evain, M., Orlandi, P. and Biagioni, C. (2012) Comparative modular analysis of two complex sulfosalt structures: sterryite, $Cu(Ag,Cu)_3Pb_{19}(Sb,As)_{22}(As\text{-}As)S_{56}$, and parasterryite, $Ag_4Pb_{20}(Sb,As)_{24}S_{58}$. *Acta Crystallographica*, **B68**, 480–492.

Nowacki, W. and Bahezre, C. (1963) Die bestimmung der chemischen zusammensetzung einiger sulfosalze aus dem Lengenbach (Binnatal, Kt. Wallis) mit Hilfe der elektronischen mikrosonde. *Schweizerische Mineralogische und Petrographische Mitteilungen*, **43**, 407–411.

Orlandi, P., Biagioni, C., Bonaccorsi, E., Moëlo, Y. and Paar, W.H. (2012) Lead-antimony sulfosalts from Tuscany (Italy). XII. Boscardinite, $TlPb_4(Sb_7As_2)_{\Sigma 9}S_{18}$, a new mineral species from the Monte Arsiccio mine: occurrence and crystal structure. *Canadian Mineralogist,* **50**, 235–251.

Orlandi, P., Biagioni, C., Moëlo, Y., Bonaccorsi, E. and Paar, W.H. (2013) Lead-antimony sulfosalts from Tuscany (Italy). XIII. Protochabournéite, ~ $Tl_2Pb(Sb_{9\text{-}8}As_{1\text{-}2})_{\Sigma 10}S_{17}$, from the Monte Arsiccio mine: occurrence, crystal structure and relationship with chabournéite. *Canadian Mineralogist*, **51**, 475–494.

Pandeli, E., Bagnoli, P. and Negri, M. (2004) The Fornovolasco schists of the Apuan Alps (Northern Tuscany, Italy): a new hypothesis for their stratigraphic setting. *Bollettino della Società Geologica Italiana*, **123**, 53–66.

Pring, A. (2001) The crystal chemistry of the sartorite group minerals from Lengenbach, Binntal, Switzerland – a HRTEM study. *Schweizerische Mineralogische und Petrographische Mitteilungen*, **81**, 69–87.

Sawada, H., Kawada, I., Hellner, E. and Tokonami, M. (1987) The crystal structure of senandorite (andorite VI): $PbAgSb_3S_6$. *Zeitschrift für Kristallographie,* **180**, 141–150.

Sheldrick, G.M. (2008) A short history of SHELX. *Acta Crystallographica*, **A64**, 112–122.

Topa, D., Makovicky, E., Tajedin, H., Putz, H. and Zagler, G. (2013) Barikaite, $Pb_{10}Ag_3(Sb_8As_{11})_{\Sigma 19}S_{40}$, a new member of the sartorite homologous series. *Mineralogical Magazine*, **77**, 3039–3046.

Wilson, A.J.C. (1992) International Tables for X-ray Crystallography Volume C. Kluwer, Dordrecht.

Table captions

Table 1. Lead sulfosalts from baryte-pyrite-iron oxide deposits from the southern Apuan Alps. Abbreviations for localities: BV = Buca della Vena mine; Fv = Fornovolasco mine; MA = Monte Arsiccio mine; Pl = Pollone mine.

Table 2. Microprobe analyses of carducciite: chemical composition as wt% and number of atoms on the basis of Σ*Me* = 16 *apfu*. Mean of 6 spot analyses.

Table 3. X-ray powder diffraction data for carducciite.

Table 4. Crystal data and summary of parameters describing data collection and refinement for carducciite.

Table 5. Atomic positions and equivalent displacement parameters for carducciite.

Table 6. Selected bond distances (Å) in carducciite.

Table 7. Bond valence calculations according to Brese and O'Keeffe (1991).

Table 8. Cell parameters of N = 4 sartorite homologues ($P2_1/c$ setting for rathite isotypes).

Table 9. Electron-microprobe chemical data of rathite and barikaite. Chemical analyses (in wt%) were recalculated on the basis of Σ*Me* = 16 *apfu*. Ev values, Pb_{corr} and $(Sb + As)_{corr}$ are calculated as in Table 2.

Table 10. Chemical variations in Ag-Pb sulfosalts from the Pollone mine

Figure captions

Fig. 1. Carducciite, black prismatic crystals up to 0.5 mm. The conchoidal fracture of carducciite is clearly visible.

Fig. 2. Crystal structure of carducciite: projection of the unit cell along **a**. Remark: for clarity, M5a (0.526 Ag) and M5b (0.474 Sb) have been represented as full grey circles, despite their partial filling.

Fig. 3. Carducciite structure: general organization. Dashed lines delimitate the N = 4 dufrénoysite-type ribbons, separated along **b** by lone-electron-pair micelles (hatched ellipses). Left: connection along **b** of Pb tricapped triangular prisms.

Fig. 4. Polymeric organization of the (Sb,As) atoms with S atoms (short bonds) in the dufrénoysite-type constitutive layer of carducciite. (a) Oblique stacking of 1D units (shaded lines); (b) ideal $Sb_3(As,Sb)_4As_2S_{20}$ polymer. No 1: with M3 mean position; No 2: first sub-choice for the two effective M3 positions; No 3: second sub-choice. Horizontal grey arrows indicate the shifts of M3 towards S8 or S9, and black double arrow the shortening of the M3 – M5b distance.

Fig. 5. Pb content (in apfu) versus (Sb + As) content (a) and Ag content (b) in the chemical formulae of members of the rathite isotypic series. Triangles = barikaite. Squares: white = carducciite; grey = rathite. Circles = ideal compositions for x = 0, 1, 1.5, and 2.

583 **Table 1.** Lead sulfosalts from baryte-pyrite-iron oxide deposits from the southern Apuan
584 Alps. Abbreviations for localities: BV = Buca della Vena mine; Fv = Fornovolasco mine; MA
585 = Monte Arsiccio mine; Pl = Pollone mine.
586
587

	Chemical formula	Localities
Lead sulfosalts		
Boulangerite	$Pb_5Sb_4S_{11}$	BdV, Fv, MA, Pl
Geocronite	$Pb_{14}Sb_6S_{23}$	Pl
Jordanite	$Pb_{14}As_6S_{23}$	Pl
Robinsonite	$Pb_4Sb_6S_{13}$	BdV, MA
Twinnite	$Pb(Sb_{0.63}As_{0.37})_2S_4$	MA, Pl
Zinkenite	$Pb_9Sb_{22}S_{42}$	BdV, MA, Pl
Lead-copper sulfosalts		
Bournonite	$CuPbSbS_3$	BdV, Fv, Pl
Jaskólskíite	$Cu_xPb_{2+x}(Sb,Bi)_{2-x}S_6$	Fv
Meneghinite	$CuPb_{13}Sb_7S_{24}$	Fv, Pl
Tintinaite	$Cu_2Pb_{10}Sb_{16}S_{35}$	BdV
Lead-iron sulfosalts		
Jamesonite	$FePb_4Sb_6S_{14}$	Fv
Lead-mercury and lead-copper-mercury sulfosalts		
Marrucciite†	$Hg_3Pb_{16}Sb_{18}S_{46}$	BdV
Rouxelite†	$Cu_2HgPb_{23}Sb_{27}S_{65.5}$	BdV, MA
Lead-silver sulfosalts		
Carducciite*†	$(Ag_2Sb_2)Pb_{12}(As,Sb)_{16}S_{40}$	Pl
Diaphorite	$Ag_3Pb_2Sb_3S_8$	Pl
Meerschautite*†	$(Ag,Cu)_6Pb_{43-2x}Sb_{44+2x}S_{112}O_x$ (x ~ 0.5)	Pl
Owyheeite	$Ag_3Pb_{10}Sb_{11}S_{28}$	Pl
Parasterryite*†	$Ag_4Pb_{20}(Sb,As)_{24}S_{58}$	Pl
Sterryite*	$Cu(Ag,Cu)_3Pb_{19}(Sb,As)_{22}(As\text{-}As)S_{56}$	Pl
Lead-thallium sulfosalts		
Boscardinite*†	$TlPb_4(Sb_7As_2)_{\Sigma 9}S_{18}$	MA
Protochabournéite*†	$Tl_2Pb(Sb_{9-8}As_{1-2})_{\Sigma 10}S_{17}$	MA
Lead oxysulfosalts, chlorosulfosalts, and oxy-chlorosulfosalts		
Dadsonite	$Pb_{23}Sb_{25}S_{60}Cl$	BdV
Pellouxite†	$(Cu,Ag)_2Pb_{21}Sb_{23}S_{55}ClO$	BdV
Pillaite†	$Pb_9Sb_{10}S_{23}ClO_{0.5}$	BdV
Scainiite†	$Pb_{14}Sb_{30}S_{54}O_5$	BdV

588 Notes: chemical formulas are from Moëlo *et al*. (2008), with the exception of sulfosalt species denoted
589 with *. Their chemical formulas are after Moëlo *et al*. (2012) [parasterryite and sterryite], Orlandi *et al*.
590 (2012) [boscardinite], Orlandi *et al*. (2013) [protochabournéite], Biagioni *et al*. (2013) [meerschautite],
591 and this work [carducciite]. The symbol † indicates sulfosalts described for the first time from the
592 baryte-pyrite-iron oxides of Apuan Alps.
593
594

595 **Table 2.** Microprobe analyses of carducciite: chemical composition as wt% and chemical
596 formula (in atoms per formula unit, *apfu*) on the basis of Σ*Me* = 16 *apfu*.
597

	1	2	3	4	5	6	mean	e.s.d.
Element	wt%	wt%	wt%	wt%	wt%	wt%	wt%	
Ag	3.58	3.33	3.52	3.63	3.55	3.66	3.55	0.12
Tl	0.11	0.13	0.12	0.12	0.18	0.12	0.13	0.03
Pb	42.62	42.15	41.55	41.69	41.56	41.84	41.90	0.42
Sb	17.82	17.56	18.13	17.77	17.78	17.67	17.79	0.19
As	12.59	12.41	12.27	12.34	12.28	12.58	12.41	0.14
S	22.37	22.23	21.98	21.98	22.06	21.96	22.10	0.17
total	99.08	97.80	97.57	97.53	97.41	97.82	97.87	0.61
	apfu	*apfu*	*apfu*	*apfu*	*apfu*	*apfu*	*apfu*	
Ag	0.960	0.905	0.955	0.985	0.970	0.990	0.961	0.031
Tl	0.015	0.020	0.015	0.020	0.025	0.015	0.018	0.004
Pb	5.945	5.975	5.870	5.895	5.895	5.880	5.910	0.041
Sb	4.230	4.235	4.360	4.275	4.295	4.225	4.270	0.052
As	4.855	4.865	4.795	4.825	4.815	4.890	4.841	0.035
S	20.410	20.370	20.075	20.085	20.225	19.940	20.143	0.147
Ev*	-0.5	-1.4	0.1	-0.2	-0.8	-0.6	-0.4	0.7
$Pb_{corr.}$**	5.975	6.015	5.900	5.935	5.945	5.910	5.947	0.043
$(Sb + As)_{corr.}$**	9.070	9.080	9.140	9.08	9.085	9.100	9.093	0.025
$Sb/(Sb + As)_{at.}$	0.465	0.465	0.476	0.470	0.471	0.464	0.469	0.005

* Relative error on the valence equilibrium (%), calculated as $[\Sigma(val+) - \Sigma(val-)] \times 100 / \Sigma(val-)$.
**$Pb_{corr.}$ and $(Sb + As)_{corr.}$ on the basis of the substitution $Tl^{+} + (As,Sb)^{3+} = 2\ Pb^{2+}$.

Table 3. X-ray powder diffraction data for carducciite.

I_{obs}	d_{meas}	I_{calc}	d_{calc}	*h k l*	I_{obs}	d_{meas}	I_{calc}	d_{calc}	*h k l*
		6	12.49	0 0 2	m	2.337	50	2.337	-2 0 10
mw	7.6	17	7.64	0 1 1	m	2.311	7	2.314	1 3 4
mw	6.8	16	6.75	0 1 2			43	2.309	2 0 8
mw	5.79	15	5.78	0 1 3			9	2.282	0 2 9
w	5.42	9	5.50	-1 0 4			25	2.254	-2 3 2
mw	4.92	19	4.93	0 1 4	**s**	**2.250**	22	2.252	2 3 0
		21	4.24	0 1 5			21	2.250	0 3 6
m	4.21	38	4.19	-2 0 2			11	2.244	-2 1 10
		17	4.18	2 0 0	vw	2.220	10	2.219	2 1 8
		17	4.03	-1 0 6	vw	2.182	5	2.185	0 1 11
m	4.01	23	4.01	0 2 0	w	2.12	65	2.122	-4 0 2
		8	3.961	0 2 1			8	2.120	0 2 10
ms	3.815	78	3.819	0 2 2	w	2.067	8	2.068	2 1 9
		6	3.802	-2 0 4	w	2.032	18	2.031	0 3 8
s	**3.689**	100	3.695	0 1 6			6	2.019	-2 2 10
		11	3.619	-1 2 1	w	1.983	11	1.980	0 4 2
ms	3.592	20	3.614	0 2 3			7	1.957	-4 1 6
		30	3.605	-2 1 3	vw	1.951	9	1.950	0 4 3
		36	3.582	2 1 1	vw	1.925	13	1.926	0 3 9
		70	3.436	-2 1 4	mw	1.912	13	1.917	-2 3 8
s	**3.416**	69	3.406	2 1 2			16	1.905	2 3 6
		8	3.375	0 2 4	vw	1.883	5	1.880	-3 3 5
vw	3.241	5	3.256	-2 0 6			6	1.858	-4 2 4
m	3.221	25	3.233	-2 1 5			10	1.852	4 2 0
		23	3.200	2 1 3	w	1.846	12	1.850	-4 1 8
s	**3.125**	67	3.128	0 2 5			9	1.848	0 2 12
		45	3.122	0 0 8			7	1.838	-2 3 9
s	**2.989**	60	3.017	-2 1 6	mw	1.833	8	1.831	4 1 4
		93	2.984	2 1 4			7	1.829	-2 1 13
		21	2.916	-2 2 1			9	1.826	2 3 7
		29	2.910	-1 1 8	w	1.810	10	1.811	2 1 11
s	**2.894**	13	2.899	-2 2 2			7	1.809	-2 4 2
		9	2.893	2 2 0			10	1.808	2 4 0
		62	2.889	0 2 6	m	1.796	14	1.800	-2 2 12
mw	2.833	13	2.845	-2 2 3			8	1.796	-2 4 3
		15	2.834	2 2 1			12	1.793	2 4 1
w	2.798	17	2.804	-2 1 7			17	1.784	2 2 10
		20	2.771	2 1 5			6	1.763	-4 2 7
vs	**2.753**	99	2.760	-2 2 4			9	1.749	4 2 3
		85	2.744	2 2 2	m	1.744	6	1.746	-3 2 11
		15	2.666	0 2 7			10	1.745	4 0 6
ms	2.657	7	2.663	-3 1 1			16	1.742	0 1 14
		12	2.659	0 3 1	mw	1.706	9	1.703	4 2 4
		16	2.651	-2 2 5	mw	1.661	7	1.659	2 4 5
		8	2.633	2 2 3	w	1.575	7	1.564	0 4 10
mw	2.632	9	2.630	3 1 0	mw	1.557	17	1.554	0 5 4
		14	2.615	0 3 2			5	1.550	-4 3 8
vw	2.462	6	2.458	0 3 4			5	1.503	0 4 11
vw	2.388	9	2.385	0 1 10					

Notes: the d_{hkl} values were calculated on the basis of the unit cell refined by using single-crystal data. Intensities were calculated on the basis of the structural model. Observed intensities were visually estimated. vs = very strong; s = strong; ms = medium-strong; m = medium; mw = medium-weak; w = weak; vw = very weak. Only reflections with I_{calc} > 5 are listed, if not observed.

658 **Table 4**. Crystal data and summary of parameters describing data collection and refinement
659 for carducciite.
660

Crystal data	
X-ray formula	$Ag_{1.05}Pb_{5.84}As_{4.63}Sb_{4.48}S_{20}$
Crystal size (mm)	0.27 x 0.16 x 0.16
Cell setting, space group	Monoclinic, $P2_1/c$
a, *b*, *c* (Å);	8.4909(3), 8.0227(3), 25.3957(9);
α, β, γ (°)	90.00, 100.382(2), 90.00
V (Å^3)	1701.63(11)
Z, Dc (g/cm^3)	2, 5.576
Data collection and refinement	
Radiation, wavelength (Å)	Mo *K*α, λ = 0.71073
Temperature (K)	293
Maximum observed 2θ	65.14
Measured reflections	17409
Unique reflections	6078
Reflections $F_o > 4\sigma(F_o)$	4137
R_{int} after absorption correction	0.0533
Rσ	0.0691
Range of *h*, *k*, *l*	$-12 \le h \le 12$, $-12 \le k \le 10$, $-33 \le l \le 38$
R [F_o>4 σ F_o]	0.0630
R (all data)	0.1026
wR (on F_o^2)	0.1460
Goof	1.107
Number of least-squares parameters	174
Maximum and minum residual peak (*e*/Å^3)	6.10 (at 0.74 Å from Pb2) -6.96 (at 0.77 Å from Pb2)

661

662 **Table 5.** Atomic positions and equivalent displacement parameters for carducciite.
663

Site	Occupancy	*x*	*y*	*z*	U_{eq} (Å^2)
Pb1	$Pb_{1.00}$	0.47837(7)	0.73364(7)	0.20441(2)	0.0330(2)
Pb2	$Pb_{1.00}$	0.97620(8)	0.73021(10)	0.20198(3)	0.0503(2)
M1	$As_{0.98(1)}Sb_{0.02(1)}$	0.29523(14)	0.83027(17)	0.34013(5)	0.0198(4)
M2	$As_{0.60(1)}Sb_{0.40(1)}$	0.24213(17)	0.31010(15)	0.14809(5)	0.0303(4)
M3	$Sb_{1.00}$	0.67428(11)	0.63675(12)	0.04195(4)	0.0288(2)
M4	$As_{0.66(1)}Sb_{0.34(1)}$	0.13884(14)	0.65000(17)	0.05807(6)	0.0314(4)
M5a	$Ag_{0.526(4)}$	0.4176(5)	0.0193(6)	0.0746(2)	0.0332(5)
M5b	$Sb_{0.474(4)}$	0.4164(5)	0.0316(6)	0.0541(2)	0.0332(5)
M6a	$Pb_{0.920(5)}$	0.90744(8)	0.07271(12)	0.07400(3)	0.0302(3)
M6b	$As_{0.080(5)}$	0.898(3)	0.013(4)	0.085(1)	0.0302(3)
S1	$S_{1.00}$	0.2596(4)	0.9911(4)	0.2658(1)	0.0227(6)
S2	$S_{1.00}$	0.2509(4)	0.4623(4)	0.2257(1)	0.0207(5)
S3	$S_{1.00}$	0.5000(4)	0.6612(4)	0.3214(1)	0.0223(6)
S4	$S_{1.00}$	0.9128(4)	0.1581(4)	0.1830(1)	0.0217(6)
S5	$S_{1.00}$	0.6880(4)	0.8348(4)	0.1153(1)	0.0230(6)
S6	$S_{1.00}$	0.1733(4)	0.8692(4)	0.1191(1)	0.0247(6)
S7	$S_{1.00}$	0.3756(4)	0.5061(4)	0.1013(1)	0.0226(6)
S8	$S_{1.00}$	0.9587(4)	0.4983(4)	0.0977(1)	0.0248(7)
S9	$S_{1.00}$	0.5942(4)	0.2000(5)	0.0098(2)	0.0306(8)
S10	$S_{1.00}$	0.1652(4)	0.1876(5)	0.0075(1)	0.0267(7)

664

665 **Table 6**. Selected bond distances (Å) in carducciite.

Pb1	– S1	2.950(3)	Pb2	– S4	2.960(3)	M1	– S4	2.236(4)	M2	– S2	2.309(3)
	– S3	2.999(3)		– S1	2.992(3)		– S1	2.262(4)		– S7	2.378(3)
	– S2	3.023(3)		– S5	3.098(3)		– S3	2.321(3)		– S3	2.492(3)
	– S7	3.183(4)		– S6	3.120(3)		– S8	3.191(4)		– S8	2.933(4)
	– S2	3.214(3)		– S2	3.149(3)		– S7	3.243(4)		– S4	3.315(3)
	– S5	3.226(3)		– S8	3.218(4)					– S6	3.639(4)
	– S6	3.250(3)		– S1	3.375(3)					– S10	3.646(4)
	– S1	3.344(3)		– S2	3.440(3)						
	– S3	3.503(3)		– S4	3.494(3)						
M3	– S5	2.435(3)	M4	– S8	2.321(4)	M5a	– S9	2.759(6)	M5b	– S9	2.446(6)
	– S7	2.458(3)		– S6	2.328(4)		– S5	2.770(5)		– S9	2.458(6)
	– S3	2.749(4)		– S7	2.405(4)		– S6	2.808(5)		– S10	2.571(6)
	– S8	2.799(3)		– S10	3.096(4)		– S9	2.819(6)		– S5	2.988(6)
	– S4	3.343(3)		– S9	3.310(4)		– S10	2.829(6)		– S6	3.149(5)
	– S6	3.634(4)					– S3	2.848(5)		– S3	3.283(5)
	– S10	3.764(4)									
M6a	– S4	2.844(3)	M6b	– S5	2.51(4)						
	– S6	2.854(3)		– S6	2.61(3)						
	– S10	2.927(4)		– S4	2.72(3)						
	– S5	2.986(3)		– S10	2.82(3)						
	– S9	3.036(4)		– S9	3.28(3)						
	– S10	3.134(3)		– S10	3.55(3)						
	– S8	3.481(4)									

666

667

Table 7. Bond valence calculations according to Brese and O'Keeffe (1991).

	Pb1	Pb2	M1	M2	M3	M4	M5a	M5b	M6a	M6b	Σ_{anions}
S1	0.34 0.12	0.30 0.11	1.01								1.88
S2	0.28 0.17	0.20 0.09		1.11							1.85
S3	0.30 0.08		0.86	0.68			0.08	0.05			2.03
S4		0.33 0.08	1.08	0.07					0.42	0.04	2.02
S5	0.16	0.23			1.04		0.10	0.11	0.28	0.06	1.98
S6	0.15	0.21				1.02	0.09	0.07	0.40	0.05	1.99
S7	0.18		0.07	0.92	0.09	0.83					2.09
S8		0.16	0.08	0.21	0.39	1.04			0.07		1.95
S9					0.45	0.07	0.10 0.09	0.47 0.46	0.25	0.01	1.90
S10					0.98	0.13	0.08	0.34	0.33 0.19	0.03	2.08
$\Sigma_{cations}$	1.78	1.71	3.10	2.99	2.95	3.09	0.54	1.50	1.94	0.19	
Theor.*	2.00	2.00	3.00	3.00	3.00	3.00	0.53	1.41	1.84	0.24	

In mixed sites, bond-valence contribution of each cation has been pondered according to its occupancy (see Table 5). * Theoretical valence on the basis of site occupancies.

692 **Table 8**. Cell parameters of N = 4 sartorite homologues ($P2_1/c$ setting for rathite isotypes).
693

Mineral	*Chemical formula*	*a* (Å)	*b* (Å)	*c* (Å)	β (°)	S.G.	Ref.
Dufrénoysite	$Pb_8As_8S_{20}$	7.90	25.74	8.37	90.35	$P2_1$	(1)
Veenite	$Pb_8(Sb,As)_8S_{20}$	8.44	26.2	7.90		unknown	(2)
Rathite	$(AgAs)Pb_6As_8S_{20}$	8.50	7.97	25.12	100.70	$P2_1/c$	(3)
Barikaite	$Ag_{1.5}Pb_5As_{5.5}Sb_4S_{20}$	8.53	8.08	24.95	100.66	$P2_1/c$	(4)
Carducciite	$(AgSb)Pb_6As_8S_{20}$	8.49	8.02	25.40	100.38	$P2_1/c$	(5)

(1) Marumo and Nowacki, 1967; (2) Jambor, 1967; (3) Berlepsch *et al*., 2002; (4) Topa *et al*., 2013; (5) this work.

694
695

696 **Table 9**. Electron-microprobe chemical data of rathite and barikaite. Chemical analyses (in
697 wt%) were recalculated on the basis of Σ*Me* = 16 *apfu*. Ev values, $Pb_{corr.}$ and $(Sb + As)_{corr.}$ are
698 calculated as in Table 2.
699

Element	1	1	1	1	2	2	2	3	4	4	4	4
	wt%	wt%	wt%	wt%	wt%	wt%	wt%	wt%	wt%	wt%	wt%	wt%
Ag	4.18	4.04	3.86	4.13	3.50	3.90	3.85	3.46	5.51	5.87	4.55	4.93
Tl	3.49	5.10	4.41	5.36	2.10	1.35	0.90	1.07	0.13	0.13	0.07	0.22
Pb	39.49	36.62	38.51	36.61	43.9	44.8	45.4	45.48	36.18	35.50	39.21	38.19
As	25.68	26.85	26.59	27.31	26.3	25.9	25.3	25.74	15.52	15.77	15.38	15.18
Sb	2.95	2.42	2.05	1.94	0.15	0.35	0.75	n.d.	18.36	18.37	16.68	17.49
Fe	0.08											
S	24.50	24.77	24.31	24.48	23.7	24.4	23.7	24.54	23.92	23.98	23.65	23.66
sum	100.37	99.80	99.74	99.82	99.17	100.6	100.00	100.29	99.62	99.63	99.55	99.68
	apfu	*apfu*	*apfu*	*apfu*	*apfu*	*apfu*	*apfu*	*apfu*	*apfu*	*apfu*	*apfu*	*apfu*
Ag	1.008	0.971	0.931	0.985	0.855	0.952	0.947	0.855	1.399	1.481	1.176	1.267
Tl	0.444	0.647	0.561	0.675	0.271	0.174	0.117	0.140	0.017	0.017	0.010	0.030
Pb	4.960	4.580	4.836	4.548	5.586	5.694	5.813	5.850	4.782	4.664	5.275	5.108
As	8.920	9.287	9.234	9.382	9.255	9.104	8.959	9.156	5.673	5.730	5.722	5.615
Sb	0.630	0.515	0.438	0.410	0.032	0.076	0.163		4.129	4.107	3.818	3.981
Fe	0.037											
S	19.883	20.019	19.725	19.649	19.487	20.039	19.610	20.395	20.428	20.358	20.557	20.448
Ev	0.8	0.4	1.8	2.1	3.0	-0.1	2.1	-1.6	-1.2	-0.9	-1.9	-1.5
$Pb_{corr.}$	5.848	5.874	5.958	5.898	6.128	6.042	6.047	6.130	4.816	4.698	5.295	5.168
$(Sb+As)_{cor.}$	9.106	9.155	9.111	9.117	9.016	9.006	9.007	9.016	9.785	9.820	9.530	9.566
$Sb/(Sb+As)_{at}$	0.066	0.053	0.045	0.042	0.003	0.008	0.018	0.000	0.421	0.418	0.400	0.415

700 1) Berlepsch *et al*., 2002; 2) Laroussi *et al*., 1989; 3) Graeser, unpubl. data, in Pring, 2001; 4) Topa *et*
701 *al*. (2013).
702
703

704 **Table 10**. Chemical variations in Ag-Pb sulfosalts from the Pollone mine.

705

	$As/(Sb+As)_{at.}$	$Pb/(Sb+As±Bi)_{at.}$	$Pb/(Ag±Cu±Tl±Hg)_{at.}$	ref.
Carducciite	0.531	0.649	6.03	[1]
Meerschautite	0.153	0.951	7.095	[2]
Owyheeite	0.099	0.924	4.361	[3]*
Parasterryite	0.391	0.859	5.329	[4]
Sb-poor sterryite	0.392	0.764	4.33	[4]
Sb-rich sterryite	0.260	0.784	4.71	[4]

706 *Average of two chemical points. [1] this work; [2] Biagioni *et al*., in prep.; [3] Carmignani *et al*. (1976);

707 [4] Moëlo *et al*., 2011;

708

709 **Fig. 1**. Carducciite, black prismatic crystals up to 0.5 mm. The conchoidal fracture of
710 carducciite is clearly visible.
711

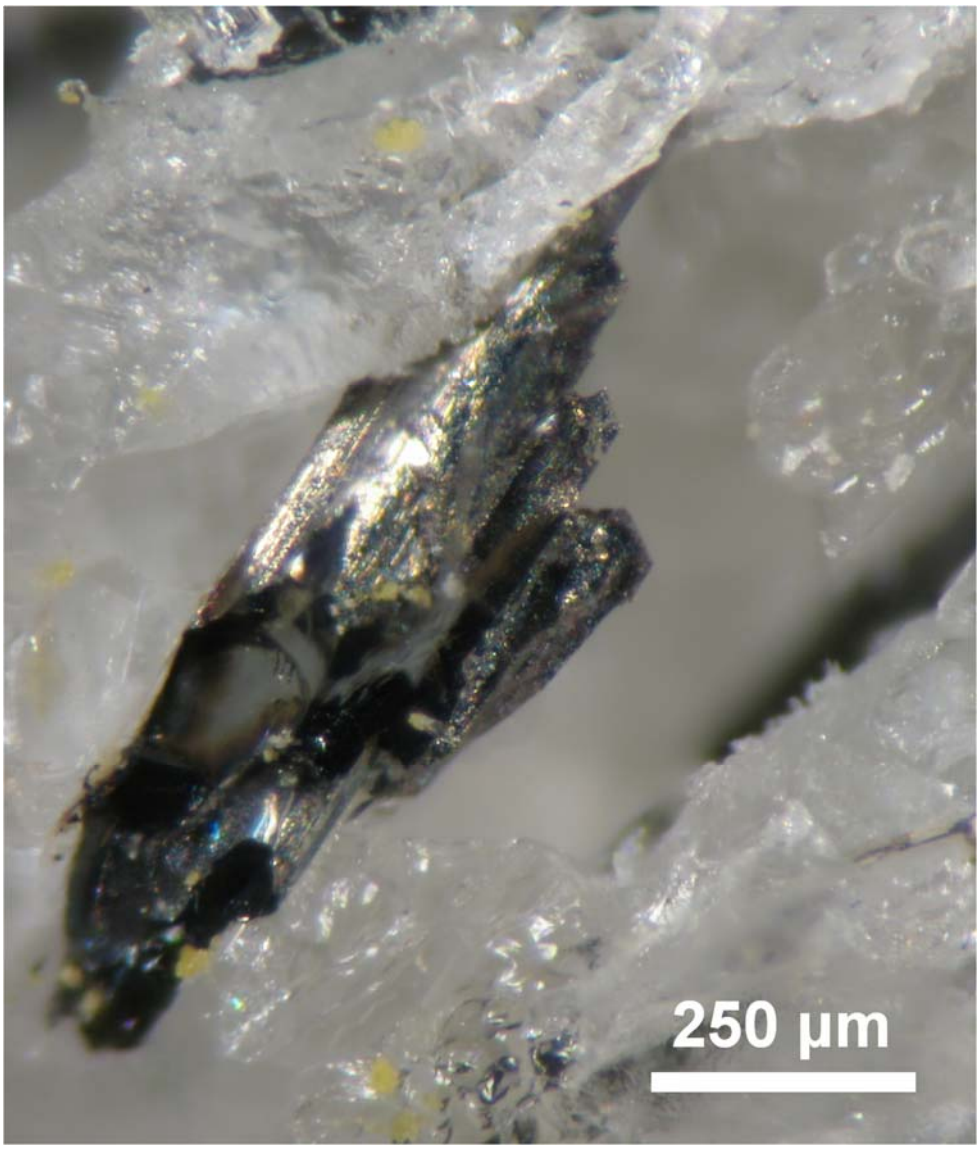

712
713
714

715 **Fig. 2**. Crystal structure of carducciite: projection of the unit cell along **a**. Remark: for clarity,
716 M5a (0.526 Ag) and M5b (0.474 Sb) have been represented as full grey circles, despite their
717 partial filling.
718

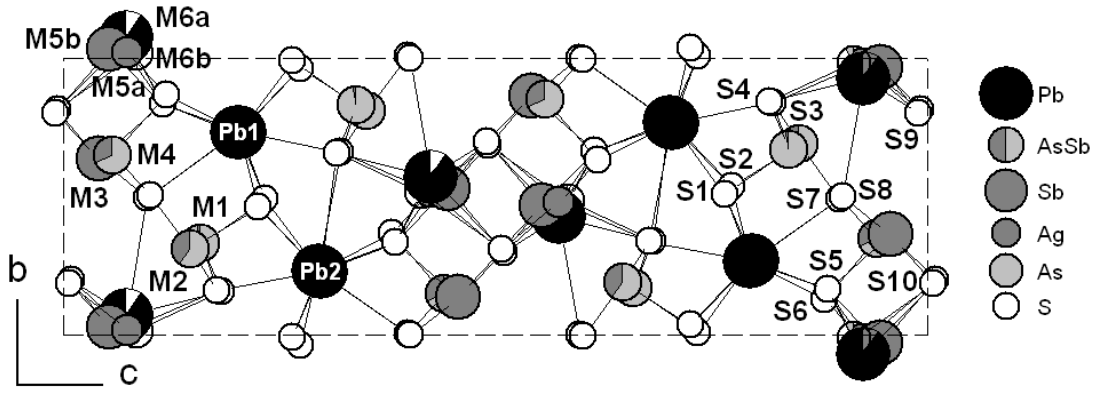

719

720 **Fig. 3**. Carducciite structure: general organization. Dashed lines delimitate the N = 4
721 dufrénoysite-type ribbons, separated along **b** by lone-electron-pair micelles (hatched ellipses).
722 Left: connection along **b** of Pb tricapped triangular prisms.
723
724

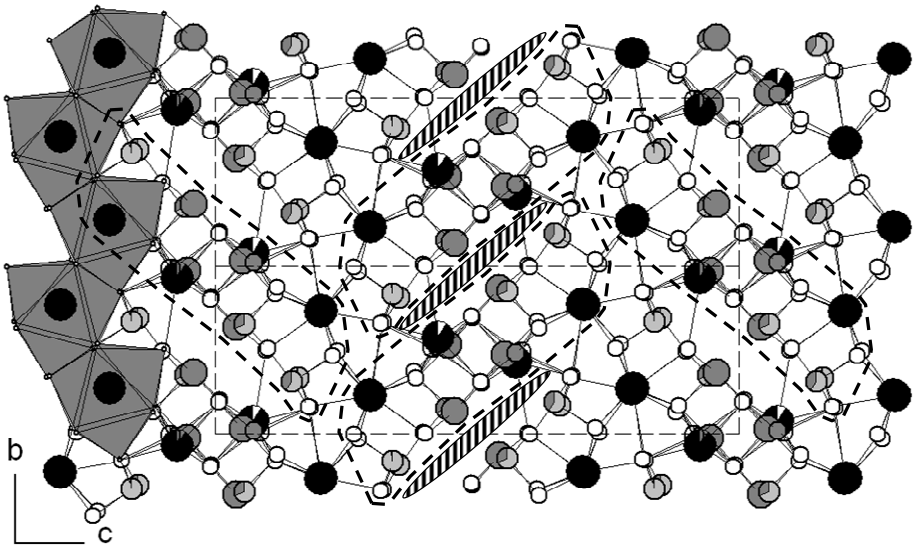

725 **Fig. 4**. Polymeric organization of the (Sb,As) atoms with S atoms (short bonds) in the
726 dufrénoysite-type constitutive layer of carducciite. (a) Oblique stacking of 1D units (shaded
727 lines); (b) ideal $Sb_3(As,Sb)_4As_2S_{20}$ polymer. No 1: with M3 mean position; No 2: first sub-
728 choice for the two effective M3 positions; No 3: second sub-choice. Horizontal grey arrows
729 indicate the shifts of M3 towards S8 or S9, and black double arrow the shortening of the M3 –
730 M5b distance.
731
732
733

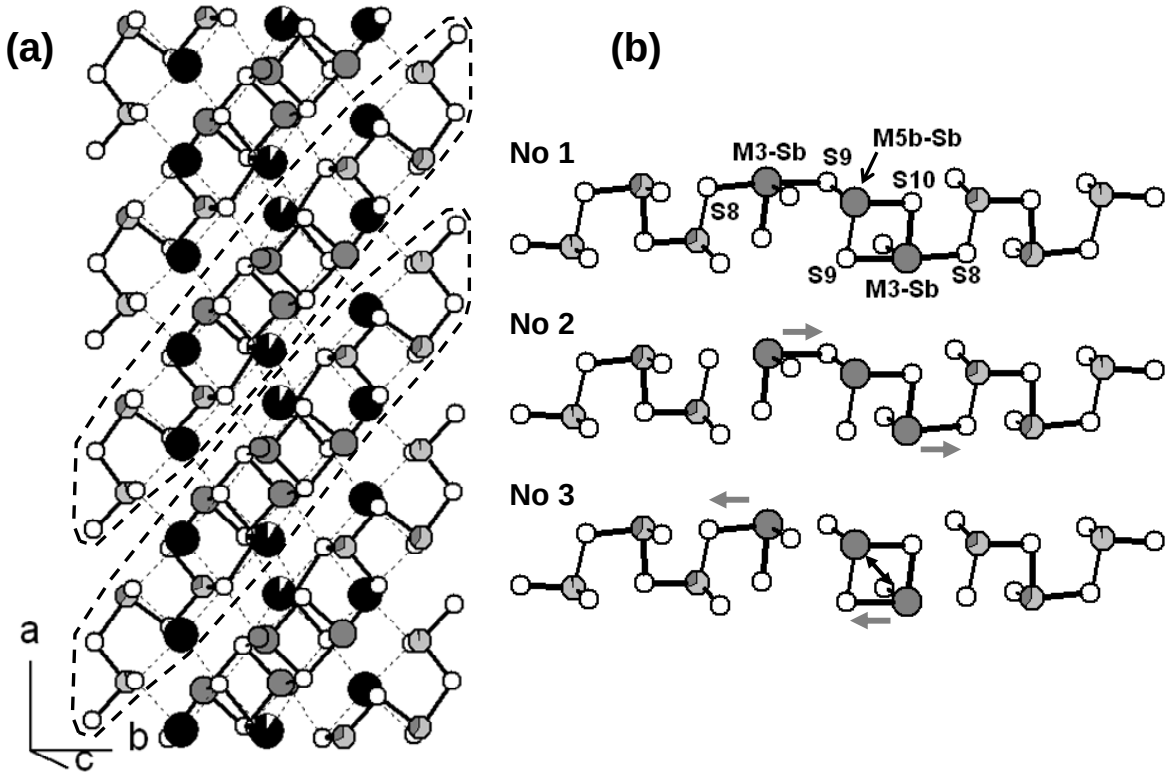

734 **Fig. 5**. Pb content (in apfu) versus (Sb + As) content (a) and Ag content (b) in the chemical
735 formulae of members of the rathite isotypic series. Triangles = barikaite. Squares: white =
736 carducciite; grey = rathite. Circles = ideal compositions for x = 0, 1, 1.5, and 2.

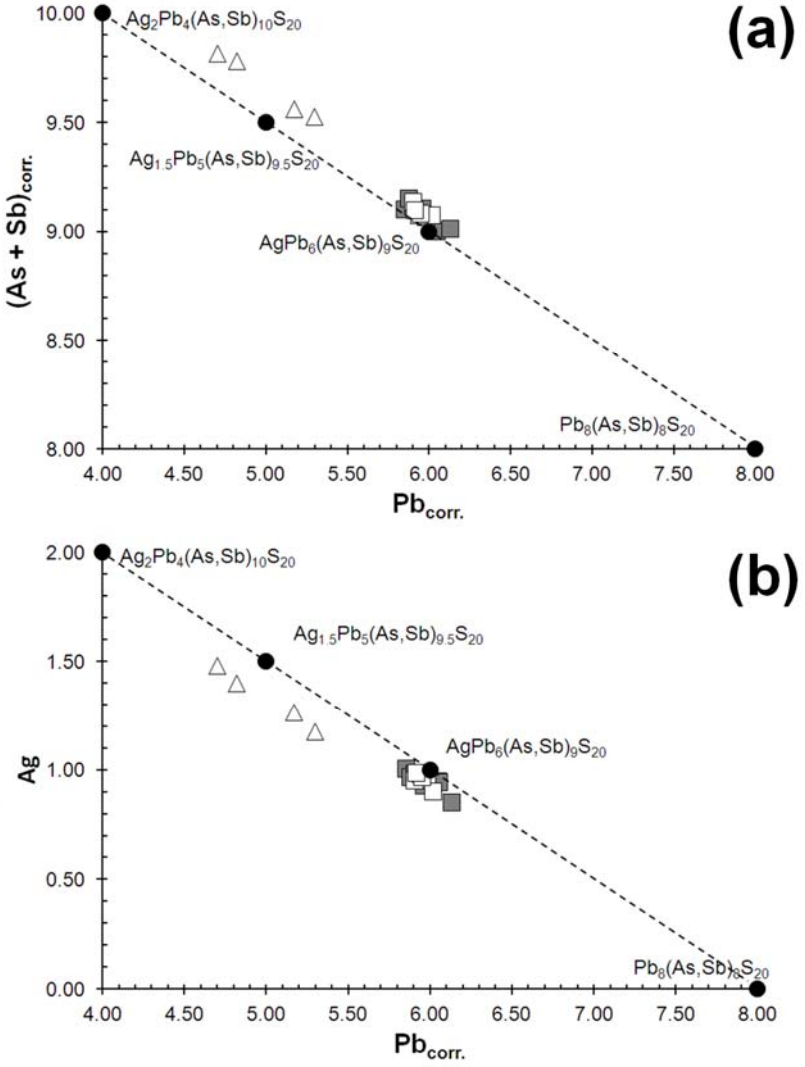

737